Testing the origin of ∼3.55 keV line in individual galaxy clusters observed with XMM-Newton

Dmytro Iakubovskyi[1], Esra Bulbul[2], Adam R. Foster[2], Denys Savchenko[1] and Valentyna Sadova[3]
[1] Bogolyubov Institute of Theoretical Physics, Metrologichna Str. 14-b, 03680, Kyiv, Ukraine
[2] Harvard-Smithsonian Center for Astrophysics, 60 Garden Street, Cambridge, MA 02138, USA
[3] Taras Shevchenko National University of Kyiv, Physics Department, Glushkova ave. 2, Kyiv, Ukraine

If the unidentified emission line at ∼3.55 keV previously found in spectra of nearby galaxies and galaxy clusters is due to radiatively decaying dark matter, one should detect the signal of comparable strength from many cosmic objects of different nature. By studying existing dark matter distributions in galaxy clusters we identified top-19 of them observed by *XMM-Newton* X-ray cosmic mission, and analyzed the data for the presence of the new line. In 8 of them, we identified $> 2\sigma$ positive line-like residuals with average position 3.52±0.08 keV in the emitter's frame. Their observed properties are unlikely to be explained by statistical fluctuations or astrophysical emission lines; observed line position in M31 and Galactic Center makes an additional argument against general-type systematics. Being interpreted as decaying dark matter line, the new detections correspond to radiative decay lifetime $\tau_{\rm DM} \approx (3.5-6)\times 10^{27}$ s consistent with previous detections.

The origin of missing mass in cosmic objects ranging from dwarf galaxies to galaxy clusters, large-scale structure and the observable part of our Universe, remains unknown. Assuming Newtonian/Einsteinian gravity and dynamics to be valid one has to introduce new type of matter – the *dark matter* – presumably in form of new elementary particles beyond the Standard Model of particle physics. Non-zero interaction strength of dark matter particles with Standard Model particles may lead to *2-body radiative decay* of the dark matter. Because present-day velocities of dark matter particles in haloes should be highly non-relativistic, such process would produce the narrow *dark matter decay line*. This motivates extensive ongoing studies of such lines in spectra of cosmic objects with established dark matter contribution.

The most intriguing dark matter decay line candidate reported so far is the ∼3.55 keV line detected in central part of the Perseus galaxy cluster and different combinations of galaxy clusters [1], Andromeda galaxy and Perseus galaxy cluster outskirts [2], Galactic Center [3], Perseus, Coma, and Ophiuchus galaxy clusters [4] [1], see also [5]. Although decaying dark matter can naturally explain basic properties of the line in these objects – correct scaling of the line signal with object redshift and projected dark matter mass density – several alternative hypotheses invoking standard or anomalously enhanced astrophysical line emission [6–8], decay of excited dark matter states [9], annihilating dark matter [10, 11], dark matter decaying into axion-like particles with further conversion to photons in magnetic field [12] have been proposed thereafter, see [5] and references therein.

To further check the decaying dark matter origin of the ∼3.55 keV line, we identified cosmic targets having the largest expected decaying dark matter signal. We used public observations of European Photon Imaging Camera (EPIC) [13, 14] on-board *XMM-Newton* X-ray observatory [15] – the most sensitive existing instrument to search narrow faint X-ray lines [16].

Object selection. For distant objects, the dark matter decay flux [$\mathrm{in\ photons\ cm^{-2}\ s^{-1}}$] is

$$F = \frac{\mathcal{S}_{\rm DM}\Omega_{\rm fov}}{4\pi m_{\rm DM}\tau_{\rm DM}}, \qquad (1)$$

where $\mathcal{S}_{\rm DM} \equiv \int \rho_{\rm DM}(l)dl$ is the dark matter column density along the line of sight, $\Omega_{\rm fov} \ll 1$ is the Field-of-View of the instrument, $m_{\rm DM}$ – mass of the dark matter particle, $\tau_{\rm DM}$ – radiative dark matter decay lifetime.

We define signal-to-noise ratio as

$$SNR = \frac{N_{line}}{\Delta N_{back}}, \qquad (2)$$

where $N_{line} \propto \mathcal{S}_{\rm DM} t_{obs}$ is the number of counts expected from decaying dark matter during observation time t_{obs} and ΔN_{back} is the uncertainty of background counts. Neglecting systematical errors and assuming Gaussian statistics, we obtained $\Delta N_{back} = \sqrt{B t_{obs}}$, where B is background count rate (in cts/s) measured in 3.4-3.65 keV in object's rest frame. So the signal-to-noise ratio is proportional to

$$SNR \propto S_{\rm DM}\sqrt{\frac{t_{obs}}{B}}. \qquad (3)$$

Because of strong dependence of SNR from $S_{\rm DM}$, we first identified objects with the largest column density in *XMM-Newton*/EPIC Field-of-View. In this paper, we concentrated on galaxy clusters – the objects having the largest column densities inside the characheristic radius of dark matter haloes [17, 18]. For each of these objects, we calculated dark matter column densities S_{obj} inside the innermost 14' radius circle R_{14} (roughly corresponding to the *XMM-Newton*/EPIC Field-of-View) using dark matter distributions

[1] Based on observed $\sim 60-100$ eV shift between line positions, [4] found improbable that their detections in Coma and Ophiuchus are of the same origin as in Perseus.

available in [17], see Appendix A, and broadened the obtained column density ranges by 0.15 dex to account typical residual uncertainties in dark matter distributions [17]. We then calculated the foreground column density $\mathcal{S}_{MW}$ from Milky Way halo by using the newest dark matter distributions compiled in [3]. Because in most of objects *XMM-Newton*/EPIC energy resolution is comparable to the energy split between the expected dark matter decay signals from object and the Milky Way halo, we multiplied the latter by a correction factor:

$$\mathcal{S}_{\rm DM} = \mathcal{S}_{obj} + \mathcal{S}_{MW} \times \exp\left(-\frac{z_{obj}^2 E_{line}^2}{2\sigma_{\rm instr}^2}\right), \qquad (4)$$

where z_{obj} is the object redshift, $E_{line} \approx 3.55$ keV is the line position, $\sigma_{\rm instr}$ is the Gaussian dispersion width corresponding to energy resolution of the instrument[2]. According to Fig. 5.24 of [19], for *XMM-Newton*/EPIC imaging spectrometers $\sigma_{\rm instr} \approx 60$ eV at the energies of our interest.

We identified 20 galaxy clusters with the largest $S_{\rm DM}$, one of them – Abell 539 – was not observed by *XMM-Newton*. The basic properties of the remaining 19 objects are summarized in Table I.

Data reduction. For objects of our interest, we first downloaded all public observation data files for MOS [13] and PN [14] cameras of *XMM-Newton* X-ray observatory [15], and processed them using *Extended Sources Analysis Software* (ESAS) package [20] publicly available as part of *XMM-Newton* Science Analysis System (SAS) v.14.0.0. Time intervals affected by highly variable background component – soft proton flares [20] – are filtered using ESAS scripts `mos-filter` and `pn-filter`. We used the standard filters and cuts provided by ESAS software. We excluded bright point sources detected with the standard SAS procedure `edetect_chain`, extracted source spectra and produced response matrices inside the 14' radius circle around the NASA Extragalactic Database (NED) source position using ESAS procedures `mos-spectra` and `pn-spectra`. Background spectra were prepared by ESAS scripts `mos_back` and `pn_back`. For PN camera, we additionally corrected the obtained spectra for out-of-time events. Finally, for each object we combined spectra and response files from MOS and PN cameras using `addspec` FTOOL procedure similar to [2, 3], and grouped the obtained spectra by 60 eV per energy bin to make the bins roughly statistically independent.

Spectral modeling. For each object, we modeled separately its combined MOS and PN spectra in `Xspec` spectral package with the sum of non-thermal (`powerlaw`) and thermal (line-free `apec`) continuum components, and several narrow `zgaussian` lines of astrophysical origin and the new line absorbed with `phabs` model and folded with response files. The `powerlaw` index $\Gamma = 1.41$ and normalization 11.6 $\rm photons\,cm^{-2}\,s^{-1}\,sr^{-1}\,keV^{-1}$ at 1 keV are fixed to best-fit values of [21]. We chose the modeled energy range 2.1-6.0 keV avoiding strong emission lines. To account residual *line-like* calibration uncertainties we added 0.4% (MOS) and 0.25% (PN) systematic errors in quadratures using `Xspec` parameter `systematic`, according to Sec. 5.3.5 of [19]. The absorption hydrogen column density was fixed at weighted Leiden-Argentine-Bonn survey [22] value obtained through $\rm n_H$ tool of the NASA High Energy Astrophysics Science Archive Research Center (HEASARC). The redshifts of `apec` and `zgaussians` were fixed at values from NASA Extragalactic Database (NED). The new line position is allowed to vary in 3.35-3.70 keV. To calculate the contribution of other astrophysical lines in this region, we used the bright 'reference' S XV line complex at $\sim$2.63 keV detected in majority of our combined spectra, see Appendix B for details.

Fit quality, plasma temperatures, maximal expected fluxes from K XVIII line complex at 3.51 keV, new line positions and normalizations, and increase of χ^2 statistics due to the new line are summarized in Table II. If no line is detected at 1σ level, we put 2σ upper bounds instead.

Discussion. Assuming decaying dark matter origin of the line at $\sim$3.55 keV previously reported by [1–4], we identified 19 galaxy clusters with the largest expected significance of dark matter decay signal. Using publicly available *XMM-Newton* observations of their central parts, we confirmed previous detections in Perseus [1, 4] and Coma [4] clusters, and found $>2\,\sigma$ positive line-like residuals in 6 new objects, see Table II for details. We consider the following traditional origins of new line detections: (a) pure statistical fluctuations; (b) contribution from nearby astrophysical emission lines; (c) (unknown) systematical effect.

To check whether pure statistical fluctuations may cause our detections, we simulated cluster spectra using FTOOL `fakeit` for all objects shown in Table II based on our best-fit models without adding a new line in 3.40-3.65 keV, looked for $\Delta\chi^2$ increase caused by adding the new narrow `zgaussian` line in the energy range 3.40-3.65 keV (thus accounting for the look-elsewhere effect). The average value of 3 maximal $\Delta\chi^2$ for each simulation is in the range 2.1-5.2, much smaller than 13.6 (12.5) obtained from our MOS (PN) observations. Therefore, we conclude that pure statistical fluctuations *alone* can not be responsible for line detections in Table II.

Explanation of the new lines with astrophysical line contribution is also unlikely. The maximal contribution of the most promising astrophysical line candidate – K XVIII line complex at $\sim$3.51 keV – is already included to our model, see Table II. Other astrophysical lines are both too faint and should produce detectable signatures at other energies. For example, to explain the excess in Virgo cluster (also consistent with

[2] For Gaussian line, the energy resolution is characterized by full width at half-maximum (FWHM) of the line which is $2\sigma\sqrt{2\log(2)} \approx 2.35\sigma_{\rm instr}$.

TABLE I: Galaxy clusters observed by *XMM-Newton* ranged by expected significance of decaying dark matter signal from their central parts.

Object	redshift	$\mathcal{S}_{\rm DM}$, M/pc^2	*XMM-Newton* ObsID	MOS/PN exposure, ks	MOS/PN SNR, arb. units
(1)	(2)	(3)	(4)	(5)	(6)
Virgo	0.0036	624-1338	0108260201, 0110930701, 0210270101	193.2 / 62.9	3.1-6.7 / 2.3-5.0
Centaurus	0.0114	818-1721	0046340101, 0406200101	348.2 / 123.7	2.9-6.0 / 2.2-4.6
Abell 85	0.0551	130-777	0065140101, 0723802101, 0723802201	401.6 / 136.7	0.6-3.8 / 0.5-2.7
Abell 478	0.0881	83-969	0109880101	111.8 / 43.2	0.3-3.5 / 0.2-2.7
Abell 2199	0.0302	123-826	0008030201, 0008030301, 0008030601, 0723801101, 0723801201	254.4 / 97.5	0.5-3.4 / 0.4-2.6
Abell 496	0.0329	124-772	0135120201, 0506260301, 0506260401	250.6 / 81.0	0.5-3.1 / 0.4-2.2
2A0335+096	0.0363	75-608	0109870101, 0109870201, 0147800201	225.2 / 89.0	0.4-2.9 / 0.3-2.4
Abell 1060	0.0126	451-1420	0206230101	66.7 / 24.7	0.9-2.8 / 0.8-2.4
Abell 3266	0.0589	385-768	0105260701, 0105260801, 0105260901, 0105261001, 0105261101, 0105262101, 0105262201, 0105262501	179.8 / 63.9	1.4-2.8 / 1.1-2.2
Abell S805	0.0139	286-660	0405550401, 0694610101	92.2 / 12.5	1.2-2.7 / 0.5-1.1
Coma	0.0231	191-1193	0124711401, 0153750101, 0300530101, 0300530301, 0300530401, 0300530501, 0300530601, 0300530701	343.8 / 122.0	0.4-2.6 / 0.3-2.1
Abell S239	0.0635	256-553	0501110201	81.0 / 28.1	0.9-1.9 / 0.6-1.3
Abell 2142	0.0909	88-573	0674560201	104.8 / 40.9	0.3-1.7 / 0.2-1.3
Abell 2319	0.0557	359-716	0302150101, 0302150201, 0600040101	159.7 / 60.7	0.8-1.5 / 0.6-1.2
Abell 1795	0.0625	83-589	0097820101	71.7 / 23.2	0.2-1.5 / 0.2-1.1
Abell 209	0.2060	67-500	0084230301	33.5 / 11.2	0.2-1.4 / 0.1-1.0
Perseus	0.0179	418-871	0085110101, 0305780101	316.4 / 44.2	0.7-1.4 / 0.3-0.7
PKS0745-191	0.1028	59-458	0105870101	31.9 / 5.2	0.1-0.8 / 0.1-0.5
Triangulum	0.0510	379-757	0093620101	18.6 / —	0.3-0.6 / —

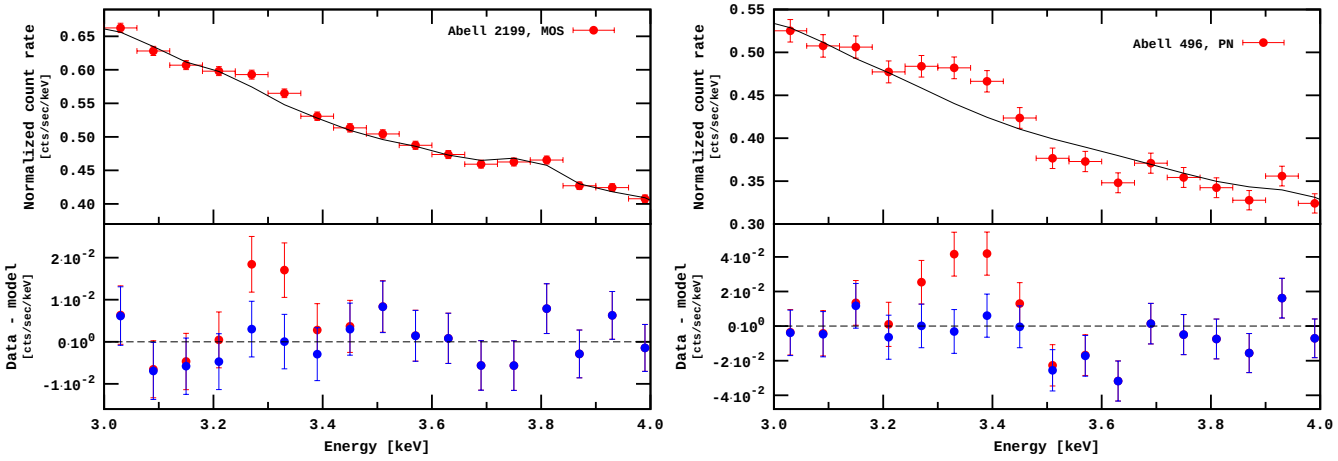

FIG. 1: Examples of spectral dataset with identified extra line, see Table II for details. The spectra are binned by 60 eV and presented in detector's frame similar to [2]. Blue and red residuals (bottom) are shown with respect to the best-fit model with and without adding an extra line, respectively. *Left:* MOS spectrum of Abell 2199. *Right:* PN spectrum of Abell 496.

pure statistical fluctuation), one should assume 3.398 keV astrophysical line from S XVI $\sim$5 times higher than the maximal contribution from the bright S XV line complex at $\sim$2.63 keV obtained from Fig. 4. On the other hand, one cannot exclude the possibility of strongly super-solar abundance because there can be variations of Potassium abudance up to 1 dex [24, 25]. According to [26], further studies of the new line using forthcoming observations of Soft X-ray spectrometer on-board *Astro-H* X-ray observatory [27] of *Micro-X* sound-

TABLE II: Model parameters of MOS/PN combined spectra of galaxy clusters listed in the previous Table. Line positions are given in cluster's rest frame. Column (4) shows our estimate on maximal K XVIII line flux at 3.51 keV using prominent S XVI line complex at 2.63 keV, see Appendix B for details. Errors on line position and flux are given at 1σ level for 2 d.o.f. calculated using $\Delta\chi^2 = 2.3$. Line fluxes are in 10^{-6}ph cm^{-2} s^{-1}, abundances are in Solar values given by [23]. The new line is detected at $> 2\ \sigma$ (corresponding to $\Delta\chi^2 > 6.2$) in 8 objects (marked in bold), confirming previous detections in Perseus [1, 4] and Coma [4].

No	Object	χ^2/d.o.f.	$T_{e,line}$, keV	max K flux at 3.51 keV	New line position, keV	New line flux	$\Delta\chi^2_{line}$
	(1)	(2)	(3)	(4)	(5)	(6)	(7)
1	Virgo	68.9/48 / 60.0/43	1.4 / 1.4	< 0.9 / < 0.7	$3.38^{+0.05}_{-0.05}$ / —	$4.2^{+3.1}_{-3.3}$ / < 9.3	3.8 / 0.4
2	Centaurus	64.1/47 / 64.3/46	2.2 / 2.2	< 5.8 / < 5.6	$3.51^{+0.12}_{-0.19}$ / —	$25.2^{+19.4}_{-24.2}$ / < 15.6	2.9 / 0.1
3	**Abell 85**	37.5/49 / 61.9/46	2.2 / 3.4	< 0.7 / < 0.9	$\mathbf{3.44}^{+0.06}_{-0.05}$ / —	$\mathbf{6.3}^{+3.9}_{-3.6}$ / < 4.2	7.0 / 0.0
4	Abell 478	54.1/47 / 48.9/49	2.2 / 1.4	< 0.4 / < 0.5	— / —	< 20.4 / < 13.6	0.1 / 0.4
5	**Abell 2199**	46.8/47 / 70.6/52	2.7 / 2.7	< 1.8 / < 1.6	$\mathbf{3.41}^{+0.04}_{-0.04}$ / —	$\mathbf{10.1}^{+5.1}_{-4.8}$ / < 10.0	10.2 / 0.1
6	**Abell 496**	36.3/45 / 66.7/48	3.4 / 2.2	< 1.3 / < 0.5	$\mathbf{3.55}^{+0.06}_{-0.09}$ / $\mathbf{3.45}^{+0.04}_{-0.03}$	$\mathbf{7.5}^{+6.1}_{-4.4}$ / $\mathbf{16.8}^{+5.9}_{-6.4}$	6.2 / 18.8
7	2A0335+096	70.9/49 / 65.3/49	2.2 / 2.7	< 1.5 / < 1.3	— / —	< 15.5 / < 10.7	0.5 / 1.6
8	Abell 1060	67.4/48 / 63.0/50	2.2 / 2.7	< 2.9 / < 1.8	— / —	< 27.1 / < 21.2	0.2 / 0.0
9	**Abell 3266**	40.7/47 / 67.2/50	1.7 / 1.7	< 0.3 / < 0.3	$3.64^{+0.05}_{-0.08}$ / $\mathbf{3.53}^{+0.04}_{-0.06}$	$6.5^{+4.3}_{-5.3}$ / $\mathbf{8.7}^{+5.1}_{-4.5}$	3.9 / 8.0
10	**Abell S805**	49.0/45 / 33.4/26	1.7 / 1.4	< 0.2 / < 0.3	— / $\mathbf{3.63}^{+0.05}_{-0.06}$	< 8.7 / $\mathbf{17.1}^{+9.3}_{-7.4}$	0.3 / 10.8
11	**Coma**	41.2/37 / 54.7/48	2.2 / 4.3	< 1.9 / < 2.0	$\mathbf{3.49}^{+0.04}_{-0.05}$ / $3.41^{+0.11}_{-0.10}$	$\mathbf{23.7}^{+10.7}_{-9.0}$ / $14.8^{+9.2}_{-9.6}$	16.6 / 3.5
12	Abell S239	56.7/48 / 60.8/52	1.4 / 1.7	< 0.1 / < 0.2	— / —	< 12.3 / < 13.6	0.3 / 0.5
13	Abell 2142	63.9/50 / 56.9/50	1.4 / 1.4	< 0.3 / < 0.3	— / —	< 9.8 / < 17.4	0.0 / 0.8
14	**Abell 2319**	49.4/47 / 61.6/51	1.4 / 2.2	< 0.4 / < 1.4	$\mathbf{3.59}^{+0.05}_{-0.06}$ / $3.53^{+0.11}_{-0.21}$	$\mathbf{18.6}^{+10.7}_{-7.4}$ / $10.5^{+12.6}_{-10.2}$	13.9 / 2.4
15	Abell 1795	61.5/51 / 64.6/50	1.7 / 1.7	< 0.3 / < 0.5	— / —	< 12.4 / < 16.5	0.7 / 0.0
16	Abell 209	62.3/50 / 68.0/48	1.4 / 1.4	< 0.5 / < 0.2	— / —	< 17.4 / < 9.4	0.6 / 0.0
17	**Perseus**	69.6/48 / 81.2/47	2.7 / 2.7	< 4.5 / < 6.1	$\mathbf{3.58}^{+0.05}_{-0.08}$ / —	$\mathbf{25.2}^{+12.5}_{-12.6}$ / < 70.4	9.8 / 0.7
18	PKS0745-191	68.9/47 / 56.0/53	2.2 / 1.4	< 0.9 / < 1.5	$3.63^{+0.07}_{-0.23}$ / —	$12.5^{+11.0}_{-12.3}$ / < 40.7	2.4 / 1.6
19	Triangulum	56.7/49 / —	2.2 / —	< 1.4 / —	— / —	< 47.1 / —	0.7 / —

ing rocket experiment [28] with superior spectral resolution $\lesssim 4-7$ eV can reveal its astrophysical origin.

The systematic origin of the new line is shown unlikely in pioneering papers [1, 2]. In addition, we plotted in Fig. 2 the dependence of the line position from the object's redshift. If the new line were due to systematic effects, one would expect the corresponding new line in nearby ($z = 0$) objects at $\sim$3.40 keV, in apparent tension with observations (3.53 ± 0.03 keV for M31 [2] and 3.539 ± 0.011 keV for Milky Way [3]) which in turn are better consistent with the new line generation in cosmic objects. The mean value of the line positions in Fig. 2 is 3.52 keV. The average spread between line positions is 75 eV close to $\sigma_{\rm instr} \approx 60$ eV and consistent with our simulations, according to that the position of $\sim 3\sigma$ line can be recovered with $\pm$110 eV precision in 90% of cases.

Interpreting the new line due to decaying dark matter (1) gives the radiative decay lifetime $\tau_{\rm DM} \approx (3-6)\times10^{27}$ s consistent with previous detections [1–4, 29], see Fig. 3. Non-detection of the line in some of our galaxy clusters does not exclude the dark matter line origin; the strongest 2σ upper bound for our objects comes from Virgo cluster: $\tau_{\rm DM} \gtrsim 3.5\times10^{27}$ s.

Non-detection of $\sim$3.55 keV line in stacked dSphs by [30] is also mildly consistent with these results; planned observations of Draco dSph would reveal the decaying dark matter nature of the line. The absence of the new line in stacked galaxy spectra of [31] formally excludes $\tau_{\rm DM} < 1.8\times10^{28}$ s but taking into account systematical effects in spectra (e.g.

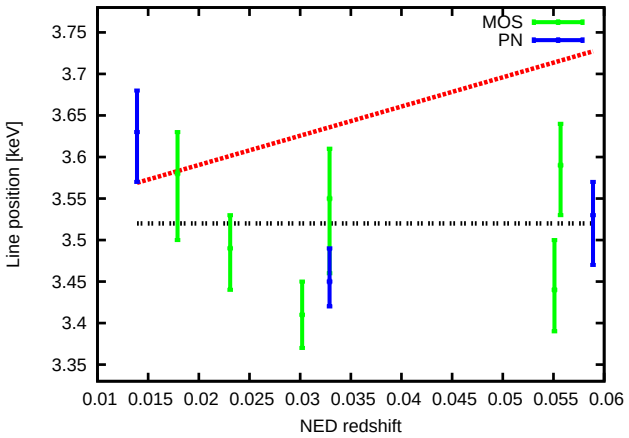

FIG. 2: Position of new line detections in cluster's rest frame as function of redshift. Only detections at $> 2\sigma$ (corresponding to $\Delta\chi^2 > 6.2$ for 2 d.o.f.) are shown. Red and black dashed lines show expected behavior in case of purely systematic and cosmic line origins (assuming line position 3.52 keV in detector's frame expected from [2, 3]), respectively.

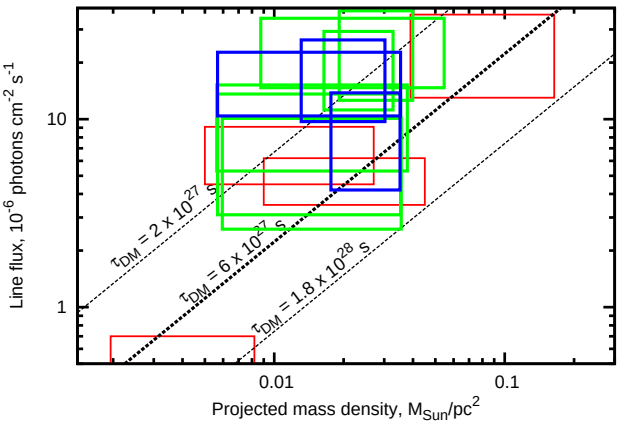

FIG. 3: Dependence of the new line flux from the expected projected dark matter mass. This Figure is taken from [3]; overplotted are the ranges for our $> 2\sigma$ MOS (green) and PN (magenta) detections. No negative detections are shown here; the strongest restriction on $\tau_{\rm DM} \gtrsim 3.5 \times 10^{27}$ s comes from Virgo cluster, see text.

causing significant negative residuals) and apparent uncertainty in dark matter distributions [17] produces much weaker bound, e.g. $\tau_{\rm DM} \gtrsim 3.5 \times 10^{27}$ s [5] using stacked dataset of nearby galaxies of [19] with comparable exposure. Other bounds on decaying dark matter in $\sim$3.55 keV energy range (see [19, 32, 33] and references therein) are also consistent with our detections after taking into account residual systematic effects and/or uncertainties of dark matter distributions.

Acknowledgments. We thank Jeroen Franse, Denys Malyshev, Maxim Markevitch and Oleg Ruchayskiy for careful reading of the manuscript and their comments. This work was supported by part by the Swiss National Science Foundation grant SCOPE IZ7370-152581, the Program of Cosmic Research of the National Academy of Sciences of Ukraine, the State Fund for Fundamental Research of Ukraine and the State Programme of Implementation of Grid Technology in Ukraine.

[1] E. Bulbul, M. Markevitch, A. Foster, R. K. Smith, M. Loewenstein, and S. W. Randall, ApJ **789**, 13 (2014), 1402.2301.
[2] A. Boyarsky, O. Ruchayskiy, D. Iakubovskyi, and J. Franse, Physical Review Letters **113**, 251301 (2014), 1402.4119.
[3] A. Boyarsky, J. Franse, D. Iakubovskyi, and O. Ruchayskiy, ArXiv e-prints (2014), 1408.2503.
[4] O. Urban, N. Werner, S. W. Allen, A. Simionescu, J. S. Kaastra, and L. E. Strigari, ArXiv e-prints (2014), 1411.0050.
[5] D. A. Iakubovskyi, Advances in Astronomy and Space Physics **4**, 9 (2014), 1410.2852.
[6] T. Jeltema and S. Profumo, MNRAS **450**, 2143 (2015), 1408.1699.
[7] T. Jeltema and S. Profumo, ArXiv e-prints (2014), 1411.1759.
[8] E. Carlson, T. Jeltema, and S. Profumo, JCAP **2**, 009 (2015), 1411.1758.
[9] J. M. Cline and A. R. Frey, Phys. Rev. D **90**, 123537 (2014), 1410.7766.
[10] E. Dudas, L. Heurtier, and Y. Mambrini, Phys. Rev. D **90**, 035002 (2014), 1404.1927.
[11] M. T. Frandsen, F. Sannino, I. M. Shoemaker, and O. Svendsen, JCAP **5**, 033 (2014), 1403.1570.
[12] P. D. Alvarez, J. P. Conlon, F. V. Day, M. C. D. Marsh, and M. Rummel, JCAP **4**, 013 (2015), 1410.1867.
[13] M. J. L. Turner, A. Abbey, M. Arnaud, M. Balasini, M. Barbera, E. Belsole, P. J. Bennie, J. P. Bernard, G. F. Bignami, M. Boer, et al., A&A **365**, L27 (2001), arXiv:astro-ph/0011498.
[14] L. Strüder, U. Briel, K. Dennerl, R. Hartmann, E. Kendziorra, N. Meidinger, E. Pfeffermann, C. Reppin, B. Aschenbach, W. Bornemann, et al., A&A **365**, L18 (2001).
[15] F. Jansen, D. Lumb, B. Altieri, J. Clavel, M. Ehle, C. Erd, C. Gabriel, M. Guainazzi, P. Gondoin, R. Much, et al., A&A **365**, L1 (2001).
[16] A. Boyarsky, J. den Herder, A. Neronov, and O. Ruchayskiy, Astroparticle Physics **28**, 303 (2007), arXiv:astro-ph/0612219.
[17] A. Boyarsky, O. Ruchayskiy, D. Iakubovskyi, A. V. Maccio', and D. Malyshev, ArXiv e-prints (2009), 0911.1774.
[18] A. Boyarsky, A. Neronov, O. Ruchayskiy, and I. Tkachev, Physical Review Letters **104**, 191301 (2010), 0911.3396.
[19] D. Iakubovskyi, Ph.D. thesis, Instituut-Lorentz for Theoretical Physics (2013).
[20] K. D. Kuntz and S. L. Snowden, A&A **478**, 575 (2008).
[21] A. De Luca and S. Molendi, A&A **419**, 837 (2004), arXiv:astro-ph/0311538.
[22] P. M. W. Kalberla, W. B. Burton, D. Hartmann, E. M. Arnal, E. Bajaja, R. Morras, and W. G. L. Pöppel, A&A **440**, 775 (2005), astro-ph/0504140.
[23] E. Anders and N. Grevesse, Geochim. Cosmochim. Acta **53**, 197 (1989).
[24] D. Romano, A. I. Karakas, M. Tosi, and F. Matteucci, A&A **522**, A32 (2010), 1006.5863.
[25] K. J. H. Phillips, B. Sylwester, and J. Sylwester, ArXiv e-prints (2015), 1507.04619.
[26] D. Iakubovskyi, ArXiv e-prints (2015), 1507.02857.
[27] K. Mitsuda, R. L. Kelley, H. Akamatsu, T. Bialas, K. R. Boyce, G. V. Brown, E. Canavan, M. Chiao, E. Costantini, J.-W. den Herder, et al., in *Society of Photo-Optical Instrumentation Engineers (SPIE) Conference Series* (2014), vol. 9144 of *Society of Photo-Optical Instrumentation Engineers (SPIE) Conference Series*, p. 2.
[28] E. Figueroa-Feliciano, A. J. Anderson, D. Castro, D. C. Goldfinger, J. Rutherford, M. E. Eckart, R. L. Kelley, C. A. Kilbourne, D. McCammon, K. Morgan, et al., ArXiv e-prints (2015), 1506.05519.
[29] M. R. Lovell, G. Bertone, A. Boyarsky, A. Jenkins, and O. Ruchayskiy, MNRAS **451**, 1573 (2015), 1411.0311.
[30] D. Malyshev, A. Neronov, and D. Eckert, Phys. Rev. D **90**, 103506 (2014), 1408.3531.
[31] M. E. Anderson, E. Churazov, and J. N. Bregman, MNRAS **452**, 3905 (2015), 1408.4115.
[32] S. Horiuchi, P. J. Humphrey, J. Oñorbe, K. N. Abazajian, M. Kaplinghat, and S. Garrison-Kimmel, Phys. Rev. D **89**, 025017 (2014), 1311.0282.

[33] N. Sekiya, N. Y. Yamasaki, and K. Mitsuda, ArXiv e-prints (2015), 1504.02826.
[34] J. F. Navarro, C. S. Frenk, and S. D. M. White, ApJ **490**, 493 (1997), arXiv:astro-ph/9611107.
[35] D. E. McLaughlin, ApJ **512**, L9 (1999), astro-ph/9812242.
[36] S. Ettori, S. De Grandi, and S. Molendi, A&A **391**, 841 (2002), astro-ph/0206120.
[37] R. Wojtak and E. L. Łokas, MNRAS **408**, 2442 (2010), 1004.3771.
[38] A. Mahdavi, H. Hoekstra, A. Babul, J. Sievers, S. T. Myers, and J. P. Henry, ApJ **664**, 162 (2007), astro-ph/0703372.
[39] E. Pointecouteau, M. Arnaud, and G. W. Pratt, A&A **435**, 1 (2005), astro-ph/0501635.
[40] K. Rines, M. J. Geller, M. J. Kurtz, and A. Diaferio, AJ **126**, 2152 (2003), astro-ph/0306538.
[41] L. M. Voigt and A. C. Fabian, MNRAS **368**, 518 (2006), astro-ph/0602373.
[42] T. Richtler, R. Salinas, I. Misgeld, M. Hilker, G. K. T. Hau, A. J. Romanowsky, Y. Schuberth, and M. Spolaor, A&A **531**, A119 (2011), 1103.2053.
[43] R. Gavazzi, C. Adami, F. Durret, J.-C. Cuillandre, O. Ilbert, A. Mazure, R. Pelló, and M. P. Ulmer, A&A **498**, L33 (2009), 0904.0220.
[44] J. Démoclès, G. W. Pratt, D. Pierini, M. Arnaud, S. Zibetti, and E. D'Onghia, A&A **517**, A52 (2010), 1005.0320.
[45] Y. Ikebe, H. Böhringer, and T. Kitayama, ApJ **611**, 175 (2004), astro-ph/0402634.
[46] N. Okabe, M. Takada, K. Umetsu, T. Futamase, and G. P. Smith, PASJ **62**, 811 (2010), 0903.1103.
[47] S. Bardeau, G. Soucail, J.-P. Kneib, O. Czoske, H. Ebeling, P. Hudelot, I. Smail, and G. P. Smith, A&A **470**, 449 (2007), astro-ph/0703395.
[48] A. Simionescu, S. W. Allen, A. Mantz, N. Werner, Y. Takei, R. G. Morris, A. C. Fabian, J. S. Sanders, P. E. J. Nulsen, M. R. George, et al., Science **331**, 1576 (2011), 1102.2429.
[49] M. R. George, A. C. Fabian, J. S. Sanders, A. J. Young, and H. R. Russell, MNRAS **395**, 657 (2009), 0807.1130.

Appendix A: Dark matter distributions in galaxy clusters

To describe dark matter distribution in galaxy clusters used in our work we compliled in Table III dark matter distributions from the literature using the extended dataset of [17].

All cluster distributions are described with Navarro-Frenk-White (NFW) profile [34]

$$\rho_{\rm NFW}(r) = \frac{\rho_s r_s}{r(1+r/r_s)^2} \tag{A1}$$

parametrised by ρ_s and r_s.

The dark matter column density inside *XMM-Newton* field-of-view radius $R_{14} = D_L \times \frac{14\pi}{60\times180}$ is derived as

$$\mathcal{S} = \frac{2}{R_{14}^2}\int_0^{R_{14}} rdr \int dz\, \rho_{\rm NFW}(\sqrt{r^2+z^2}) \tag{A2}$$

For the NFW density distribution (A1):

$$\mathcal{S}_{\rm NFW}(R) = \frac{4\rho_s r_s^3}{R^2}\left[\frac{\arctan\sqrt{R^2/r_s^2-1}}{\sqrt{R^2/r_s^2-1}} + \log\left(\frac{R}{2r_s}\right)\right] . \tag{A3}$$

Dark matter distribution parameters for our Galaxy are taken from [3].

Appendix B: Modeling astrophysical lines

To check the astrophysical origin of the new line, we added narrow `zgaussians` corresponding to known astrophysical lines in this range. For example, according to the newest atomic database AtomDB v. 3.0.3, there are S XVI line complexes at 3.355, 3.398, 3.424, 3.441, 3.452 and 3.460 keV. Fortunately, the intensity of these lines can be robustly predicted by the measured S XV line complex at $\sim$2.63 keV, see Fig. 4 for details.

We paid special attention to potential contribution from K XVIII lines near 3.51 keV, see e.g. [26] for details. The distance between these lines is smaller than the energy resolution of *XMM-Newton*/EPIC, so we modeled the K XVIII line complex as a

Object	Reference	Profile	R_{14} kpc	r_s kpc	ρ_s $10^6 M_\odot/\mathrm{kpc}^3$	$\mathcal{S}_{obj}$ $M_\odot/\mathrm{pc}^2$
Virgo	[35]	NFW	73	560	0.32	808
Centaurus	[36]	NFW	180	345	1.51	1087
Abell 85	[36]	NFW	867	1282	0.25	549
Abell 85	[37]	NFW	922	650	0.37	210
Abell 478	[38]	NFW	1978	1140	0.85	686
Abell 478	[39]	NFW	1518	488	0.77	134
Abell 2199	[36]	NFW	526	560	0.76	552
Abell 2199	[40]	NFW	509	214	1.7	180
Abell 496	[36]	NFW	545	738	0.45	530
Abell 496	[37]	NFW	550	420	0.48	191
2A0335+096	[36]	NFW	593	626	0.52	420
2A0335+096	[41]	NFW	593	130	3.6	101
Abell 1060	[42]	NFW	195	140	7.2	899
Abell 1060	[37]	NFW	211	140	5.8	667
Abell 3266	[36]	NFW	991	1576	0.19	543
Abell S805	[37]	NFW	232	190	2.0	386
Coma	[36]	NFW	397	459	1.23	788
Coma	[43]	NFW	407	326	0.85	275
Abell S239	[44]	NFW	1095	792	0.55	391
Abell S239	[44]	NFW	1095	576	0.98	361
Abell 2142	[36]	NFW	1469	1654	0.18	406
Abell 2142	[37]	NFW	1520	990	0.18	144
Abell 2319	[36]	NFW	943	1301	0.24	506
Abell 1795	[36]	NFW	1052	1024	0.34	417
Abell 1795	[45]	NFW	1052	393	0.82	139
Abell 209	[46]	NFW	3460	2513	0.18	408
Abell 209	[47]	NFW	3435	502	0.386	24
Perseus	[48]	NFW	305	360	1.1	563
PKS 0745-191	[36]	NFW	1665	1148	0.33	324
PKS 0745-191	[49]	NFW	1779	230	2.5	59
Triangulum	[36]	NFW	856	666	0.83	534

TABLE III: Parameters of dark matter distributions of galaxy clusters used in this work.

single `zgaussian` with mean energy 3.51 keV. Because there is no "reference" Potassium line to reproduce the 3.51 keV line flux, we fixed only the upper bound of the 3.51 keV line intensity relating it to S XVI line flux at 2.63 keV (or, if 2.63 keV is not detected in the dataset – to its 2σ upper bound) using the procedure described in [26]. To derive electron temperature, we used flux ratios of strong elemental lines, namely S XV lines at 2.45 keV, S XVI lines at 2.63 keV, Ca XIX lines at 3.90 keV and Ca XX lines at 4.10 keV. Because 3.51/2.63 keV line ratio is a decreasing function of electron temperature T_e, see Fig. 4, we used minimal temperature $T_{e,line} = \min[T_{e,S}, T_{e,Ca}]$ for conservative estimate. Another source of uncertainty comes from the (largely unknown) relative K/S abundance ratio. To account possible uncertainties [6, 24, 25] we allowed this ratio to be up to 3 Solar values of [23]. Note that from comparison of columns 4 and 6 one can derive that to explain new line emission solely in terms of K XVIII line complex at 3.51 keV, one should assume strongly supersolar (Abund[K]/Abund[S] $>$15 Solar) ratios for *all* our of detections.

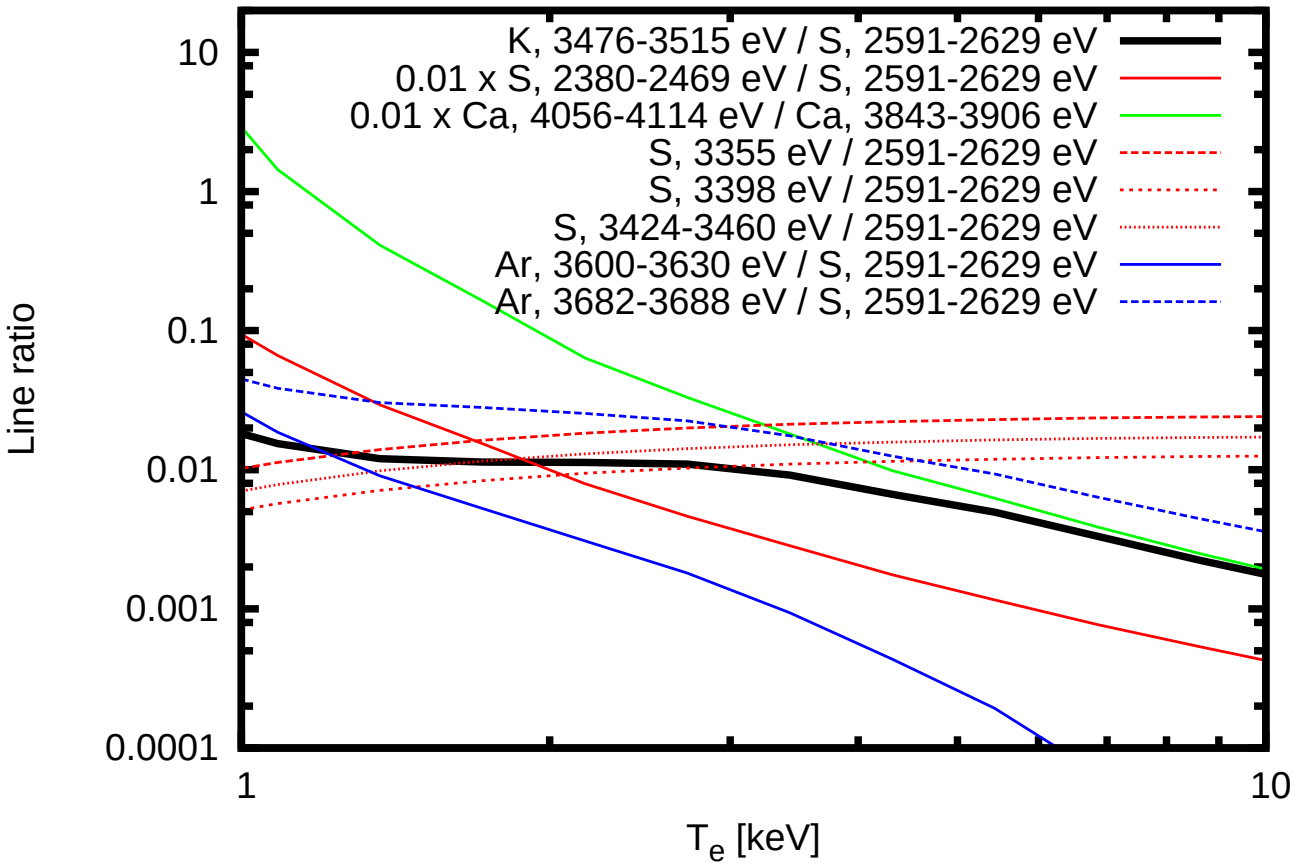

FIG. 4: Line emissivity ratios for K XVIII line complex at ∼3.51 keV and other emission lines of our interest as functions of the electron temperature T_e in the plasma. The line emissivities are calculated using AtomDB version 3.0.3 with line emissivities $> 10^{-22}$ ph cm^3/s.